Electronic Supplementary Information (ESI)

Acceleration of the pre-oxidation process by tuning the degree of sulfurization for promoted oxygen evolution reaction

Junfeng Xie[†,*] Changgang Dong,[†] Jiechen Li, Min Guo, Ying Zhao, Luyao Kang, Wen Gao, Fengcai Lei, and Bo Tang[*]

College of Chemistry, Chemical Engineering and Materials Science, Key Laboratory of Molecular and Nano Probes (Ministry of Education), Collaborative Innovation Center of Functionalized Probes for Chemical Imaging in Universities of Shandong, Institute of Molecular and Nano Science, Shandong Normal University, Jinan, Shandong, 250014, P. R. China. E-mail: xiejf@sdnu.edu.cn; tangb@sdnu.edu.cn.

† These authors contributed equally to this work.

1. Experimental section

1.1 Synthesis of ZIF-67 and Co-N-C

Typically, 0.874 g $Co(NO_3)_2 \cdot 6H_2O$ (3 mmol) was dissolved in 30 mL methanol (MeOH) to form a transparent solution. Afterwards, 0.985 g 2-methylimidazole (2-MeIm; 12 mmol) was dissolved in 10 mL MeOH. Then, the solution of 2-MeIm was subsequently injected into the solution of $Co(NO_3)_2 \cdot 6H_2O$. After stirring at room temperature for 48 h, purple precipitates were collected by centrifugation, washed with MeOH for several times and dried at 40 ºC under vacuum to obtain ZIF-67. The as-obtained ZIF-67 was heated to 900 ºC in a tube furnace at a heating rate of 5 ºC min^{-1} under Ar atmosphere and maintained for 2 h to obtain the Co-N-C.

1.2 Synthesis of the Co-based catalysts encapsulated in porous N-doped carbon with variable degrees of sulfurization

The sulfurized Co-based catalysts were prepared by a hydrothermal method. For the synthesis of the partially sulfurized Co_3S_4/Co-N-C, 100 mg Co-N-C was dispersed in 80 mL deionized water by ultrasonication, then 0.7513 g thioacetamide (TAA; 10 mmol) was added and dissolved by vigorous stirring for 10 min. The mixture was then transferred into a 100 mL Teflon-lined stainless-steel autoclave, and maintained at 140 ºC for 12 h. After that, the reaction system was allowed to cool to room temperature naturally. The as-obtained powdery product (Co_3S_4/Co-N-C) was washed with deionized water and ethanol for several times, and then dried in vacuum at 40 ºC. By simply changing the reaction temperatures of the hydrothermal treatment, the surface sulfurized Co-N-C/S (60 ºC) and fully sulfurized Co_3S_4/N-C (200 ºC) can be fabricated.

1.3 Structural characterizations

The X-ray diffraction (XRD) was performed on a Philips X'Pert Pro Super diffractometer with Cu Kα radiation (λ = 1.54178 Å). The Raman spectroscopy was performed with a laser micro-Raman spectrometer (Horiba LabRAM HR Evolution, 532 nm excitation wavelength). The scanning electron microscopy (SEM) images were taken on a JEOL JSM-6700F SEM. The transmission electron microscopy (TEM) was carried out on a JEM-2100F field emission electron microscope at an acceleration voltage of 200 kV. The

high-resolution TEM (HRTEM), high-angle annular dark-field scanning transmission electron microscopy (HAADF-STEM) and corresponding elemental mapping analyses were performed on a Thermo Fischer Talos F200X TEM. The nitrogen adsorption-desorption isotherms were carried out by using a Micromeritics ASAP 2460 system, and all the gas adsorption experiments were performed at liquid-nitrogen temperature (77 K) after degassed at 300 °C for 6 h. The atomic ratio of Co:S was determined by inductively coupled plasma optical emission spectrum (ICP-OES) on a Perkin Elmer Optima 7300DV ICP emission spectroscope. The X-ray photoelectron spectroscopy (XPS) analyses were performed on a VGESCALAB MKII X-ray photoelectron spectrometer with an excitation source of Mg Kα = 1253.6 eV, and the resolution level was lower than 1 atom%.

1.4 Electrocatalytic study

All the electrochemical measurements were performed in a three-electrode system linked with an electrochemical workstation (Ivium Vertex. C. EIS). All potentials were calibrated to a reversible hydrogen electrode (RHE) according to the Nernst equation and the data were presented without iR correction. Typically, 4 mg of catalyst and 50 μL Nafion solution (Sigma Aldrich, 5 wt%) were dispersed in 1 mL water-isopropanol mixed solution (volume ratio of 3:1) by sonicating for at least 30 min to form a homogeneous ink. Then 5 μL of the dispersion (containing 20 μg of catalyst) was loaded onto a glassy carbon electrode with 3 mm diameter, resulting in a catalyst loading of 0.285 mg cm^{-2}. The as-prepared catalyst film was allowed to be dried at room temperature. The cyclic voltammetry (CV) and linear sweep voltammetry (LSV) with a scan rate of 2 mV s^{-1} were conducted in O_2-purged 1 M KOH solution. A Hg/HgO electrode was used as the reference electrode, a platinum gauze electrode (2 cm × 2 cm, 60 mesh) was used as the counter electrode, and the glassy carbon electrodes loaded with various catalysts were served as the working electrodes. The Faradaic efficiency (FE) was calculated from the volume of the as-generated O_2 gas at a constant anodic current of 20 mA by using chronoamperometric method. The electrochemical impedance spectroscopy (EIS) measurements were operated in the same configuration at 1.6 V vs. RHE from 10^{-2}-10^{5} Hz.

2. Additional physical and electrochemical characterizations

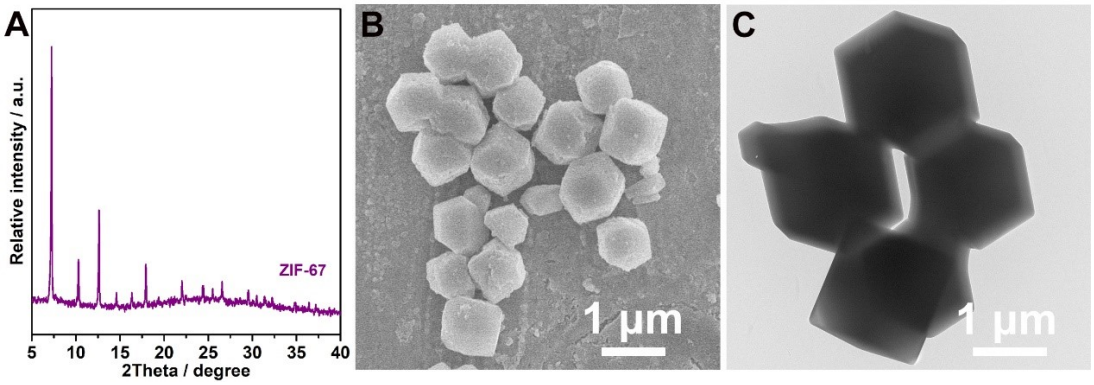

Fig. S1 (A) XRD pattern, (B) SEM image and (C) TEM image of the ZIF-67 precursor. ZIF-67 exhibits typical rhombic dodecahedral shape with size of 1 μm.

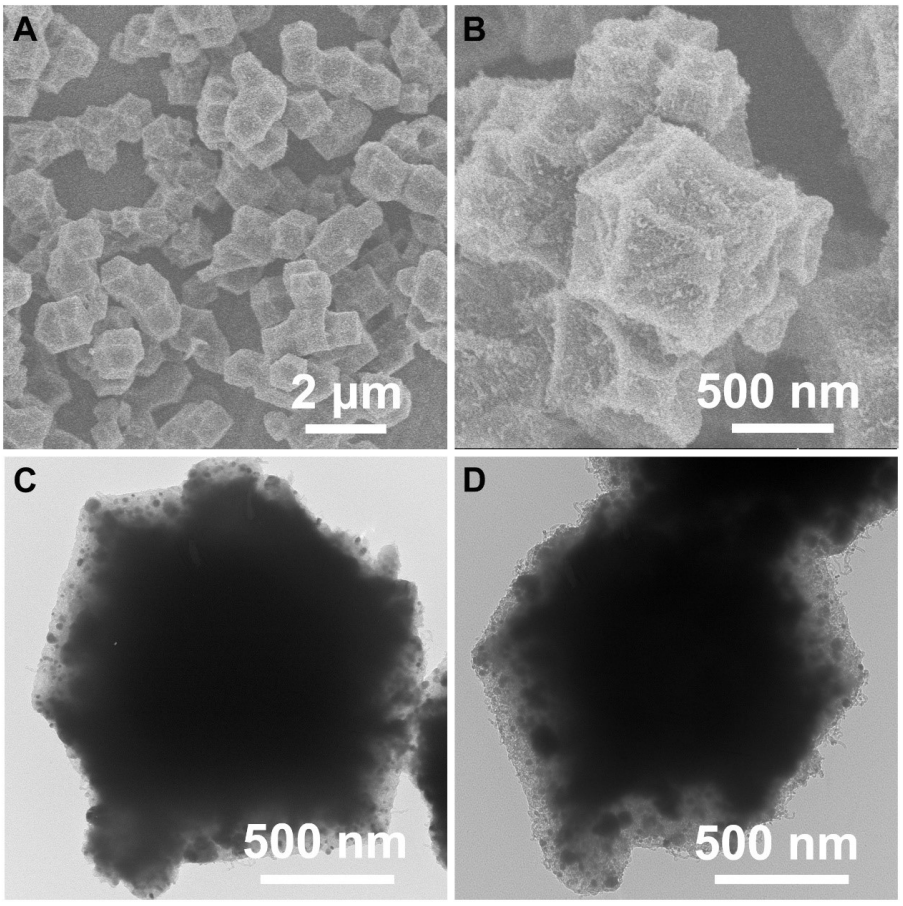

Fig. S2 (A-B) SEM and (C-D) TEM images of the pristine Co-N-C. After the pyrolysis of ZIF-67, Co-N-C with rhombic dodecahedral morphology can be formed.

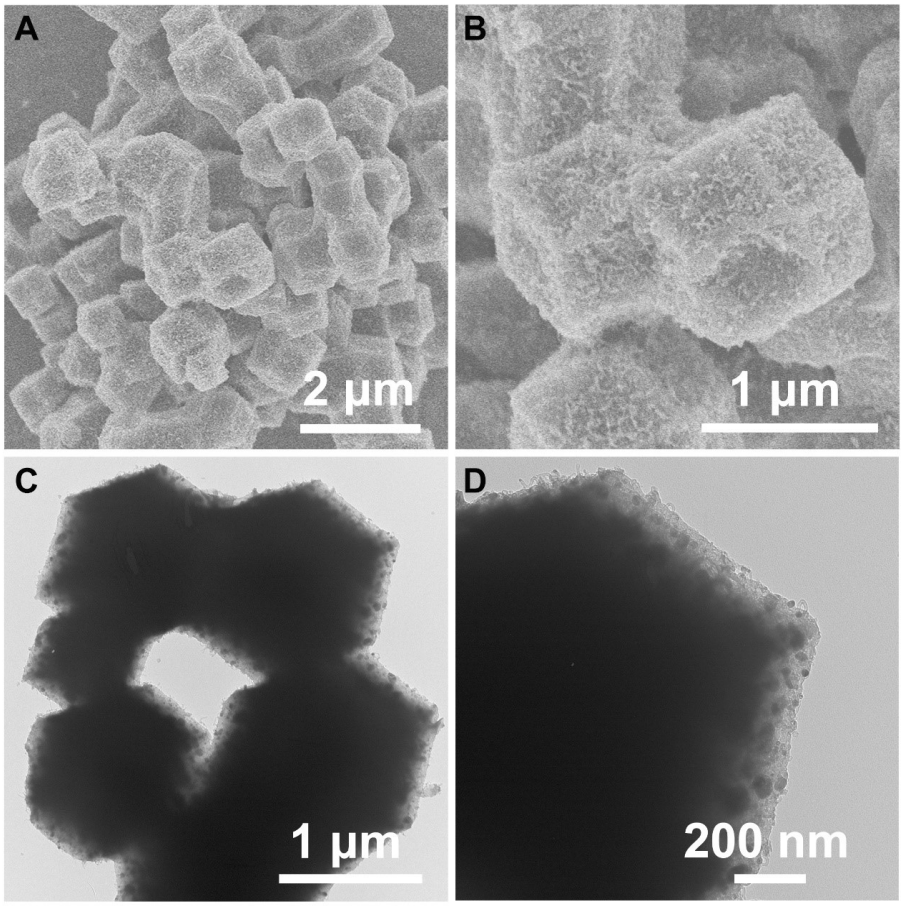

Fig. S3 (A-B) SEM and (C-D) TEM images of the surface sulfurized Co-N-C/S (low DoS). Negligible difference in morphology can be observed for the surface sulfurized Co-N-C/S compared with the Co-N-C.

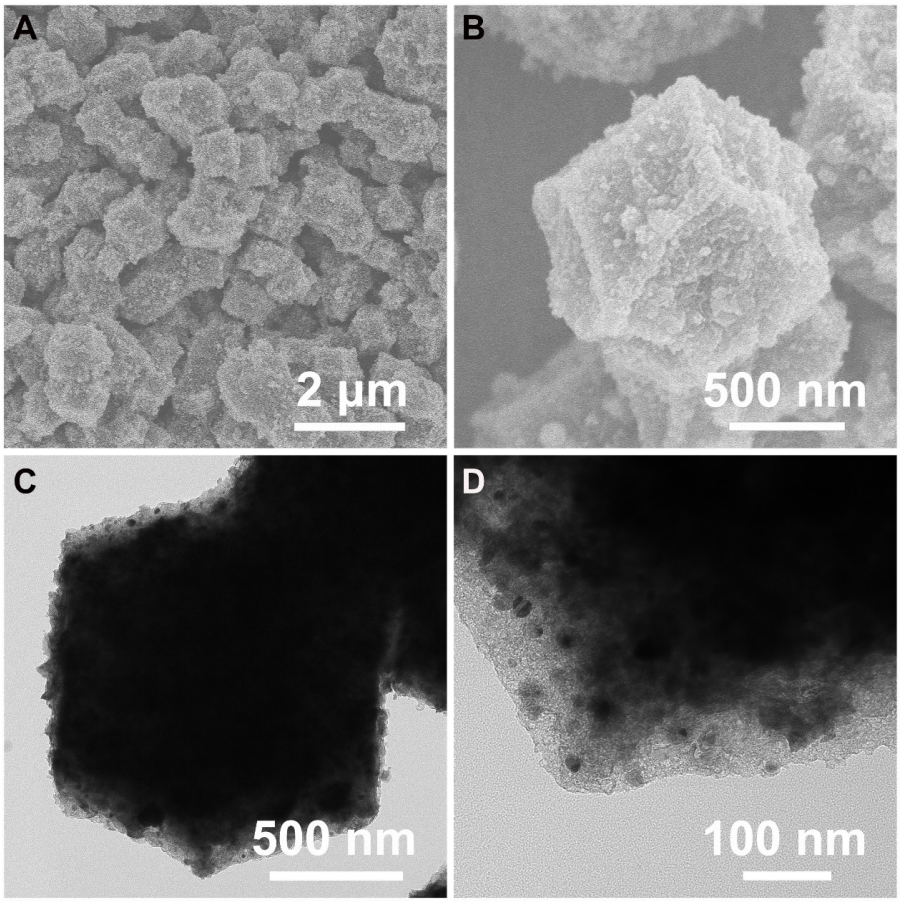

Fig. S4 Additional SEM (A-B) and TEM (C-D) images of the partially sulfurized Co_3S_4/Co-N-C hybrid catalyst (medium DoS).

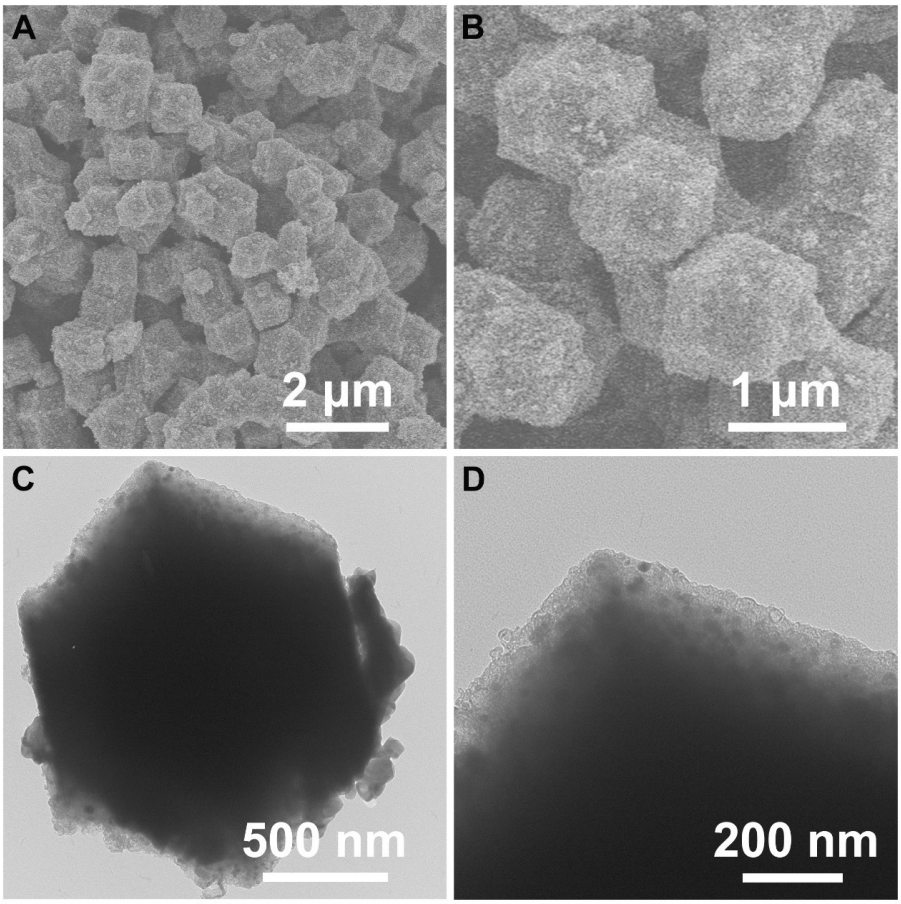

Fig. S5 (A-B) SEM and (C-D) TEM images of the fully sulfurized Co_3S_4/N-C (high DoS).

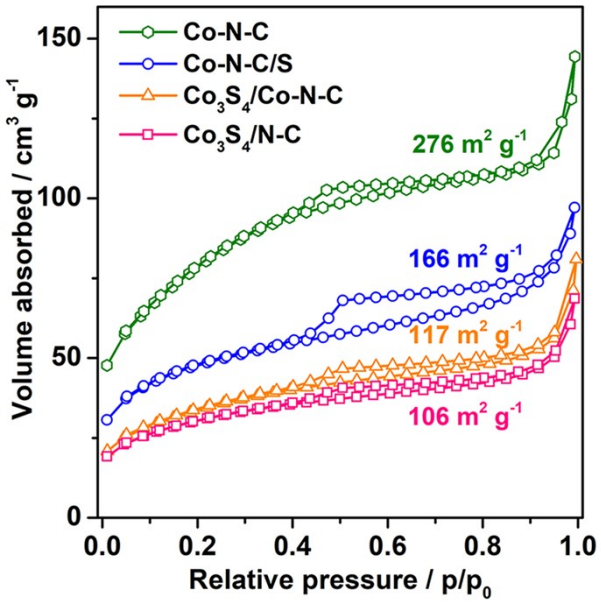

Fig. S6 Nitrogen adsorption/desorption isotherms with BET specific surface areas.

As can be seen from the ICP-OES results in Table S1, the DoS of the partially

sulfurized Co-based nanocatalysts can be well controlled. The atomic ratio of Co:S exhibits gradual increment with the increased amounts of the added TAA reactant, indicating the increased content of the Co_3S_4 component. As shown in Table S1, the partially sulfurized Co_3S_4/Co-N-C catalyst displays a Co:S atomic ratio of 1.00:0.78. Considering the stoichiometry of Co_3S_4 with Co:S atomic ratio of 3:4, 58.5% Co in Co-N-C was transformed into Co_3S_4 during the hydrothermal sulfurization, and the molar ratio of Co_3S_4:Co is determined to be 1.00:2.13. For the surface sulfurized Co-N-C/S, a lower Co:S ratio of 1.00:0.18 can be resulted, and approximately 13.5% Co was transformed into sulfides. Of note, owing to the amorphous nature of the sulfide species in Co-N-C/S, this value can only be regarded as a reference. Furthermore, the fully sulfurized Co_3S_4/N-C catalyst exhibits a high Co:S ratio of 1.00:1.36, and the content of S is even slightly higher than that for Co_3S_4, suggesting the complete phase transformation from Co to Co_3S_4. The excess S species may originate from the adsorption of S-containing ions on the N-C skeleton.

Table S1 The ICP-OES results of the sulfurized Co-based nanocatalysts.

Materials	Atomic ratio of Co:S	Percentage of Co transformed into sulfides
Co-N-C/S	1.00:0.18	13.5%
Co_3S_4/Co-N-C	1.00:0.78	58.5%
Co_3S_4/N-C	1.00:1.36	100%

X-ray photoelectron spectroscopy (XPS) was conducted to further survey the compositional and valence information of the as-obtained Co-based catalysts. As shown in the survey spectra in S7-10, Co, C, N and O can be detected for all the samples, and the presence of S species can be verified for the sulfurized catalysts with variable DoS. Taking the partially sulfurized Co_3S_4/Co-N-C as an example, the Co 2p spectrum in Fig. S9B can be deconvoluted as two sets of peaks corresponding to the Co $2p_{3/2}$ and Co $2p_{1/2}$ orbitals. As can be seen, the deconvoluted peaks in Co $2p_{3/2}$ region with triple peaks located at 779.7, 781.9 and 778.8 eV can be indexed as the Co^{3+}, Co^{2+} and Co^0 species, and the peaks in Co $2p_{1/2}$ region centered at 794.8, 797.8 and 793.9 eV can also be

assigned to the Co^{3+}, Co^{2+} and Co^{0} species, respectively.[1, 2] In addition, the broad signals at 803.3 eV and 786.6 eV can be ascribed to the satellite peaks.[1-3] Hence, mixed valence of Co species can be confirmed, which can be attributed to the hybrid feature of the Co_3S_4/Co nanocrystals. Similar to the partially sulfurized Co_3S_4/Co-N-C hybrid catalyst, the surface sulfurized Co-N-C/S and Co-N-C also exhibits mixed valence of Co^{3+}, Co^{2+} and Co^{0} (Fig. S7B and 8B), for which the oxidized Co species can be attributed to the surface oxidation of the Co nanocrystals during the hydrothermal sulfurization treatment. In contrast, no Co^{0} species can be detected for the fully sulfurized Co_3S_4/N-C (Fig. S10B), indicating the complete phase transformation from Co to Co_3S_4, which is consistent with the result from XRD analyses. To study the chemical states of sulfur in the sulfurized catalysts, the high-resolution S 2p spectra were analyzed. As shown in the S 2p spectrum of the partially sulfurized Co_3S_4/Co-N-C in Fig. S9C, the dominance of S^{2-} species can be identified, for which the classical single doublet peak at 162.1 eV demonstrates the formation of metal sulfides.[3] In addition, the weak peaks located at 163.8 and 169.0 eV can be assigned to the C-S bonds and SO_4^{2-} species in the sample,[4] which are originated from the catalyst anchoring and surface oxidation, respectively. Similar to the S 2p spectrum of the partially sulfurized Co_3S_4/Co-N-C, the abovementioned S species can also be observed for the surface sulfurized and fully sulfurized catalysts (Fig. S8C and 10C). Besides, the XPS spectra of C and N of the partially sulfurized Co_3S_4/Co-N-C are shown in Fig. S9D-E. As can be seen, the deconvolved C 1s peaks at 284.7, 285.5, 286.5, 288.6 and 290.9 eV can be indexed as the C-C, C=N, C-O, C=O and C=C groups, respectively,[5, 6] therefore confirming the dominance of the sp^2-hybridized carbon with nitrogen doping and oxygen-containing functional groups. In addition, the N 1s XPS spectrum in Fig. S9E further verifies the nitrogen doping in the porous carbon skeleton. As can be seen, three types of N atoms can be identified, where the peaks at 399.0 and 401.5 eV can be assigned to the pyridinic N and graphitic N, while the dominant peak located at 400.5 eV can be designated as the pyrrolic N, respectively.[5, 7] As reported previously, the N doping in sp^2-hybridized carbon could not only facilitate the intimate anchoring of the nanocatalysts,[1, 8] but also improve the charge transfer behavior owing to the effective electron injection from N atoms to the carbon conjugated system.[9] In

addition, three deconvoluted peaks can be observed for the O 1s spectrum. As shown in Fig. S9F, the weak peak at 531.3 eV can be assigned to the hydroxyl groups on the surface of the Co-based nanocrystals, and the intensive peaks at 532.2 and 533.1 eV can be attributed to the adsorbed water and C-O species, respectively.[10]

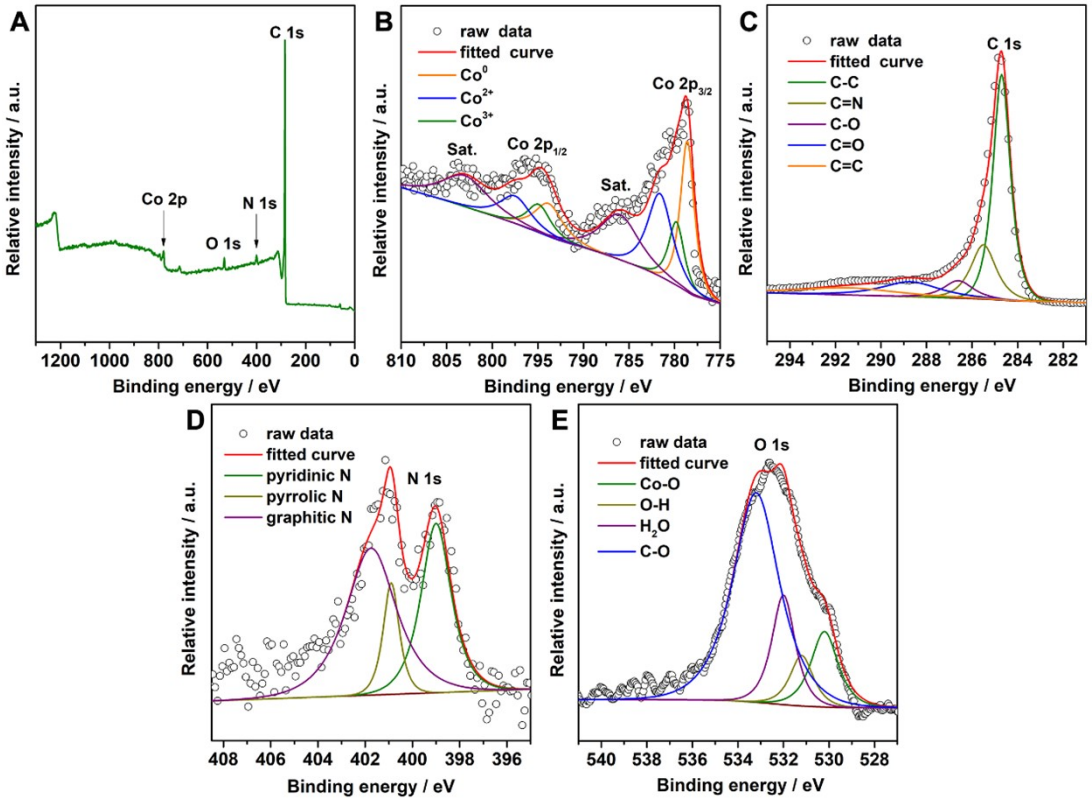

Fig. S7 (A-E) XPS survey spectrum and the high-resolution spectra of Co, C, N and O of the pristine Co-N-C.

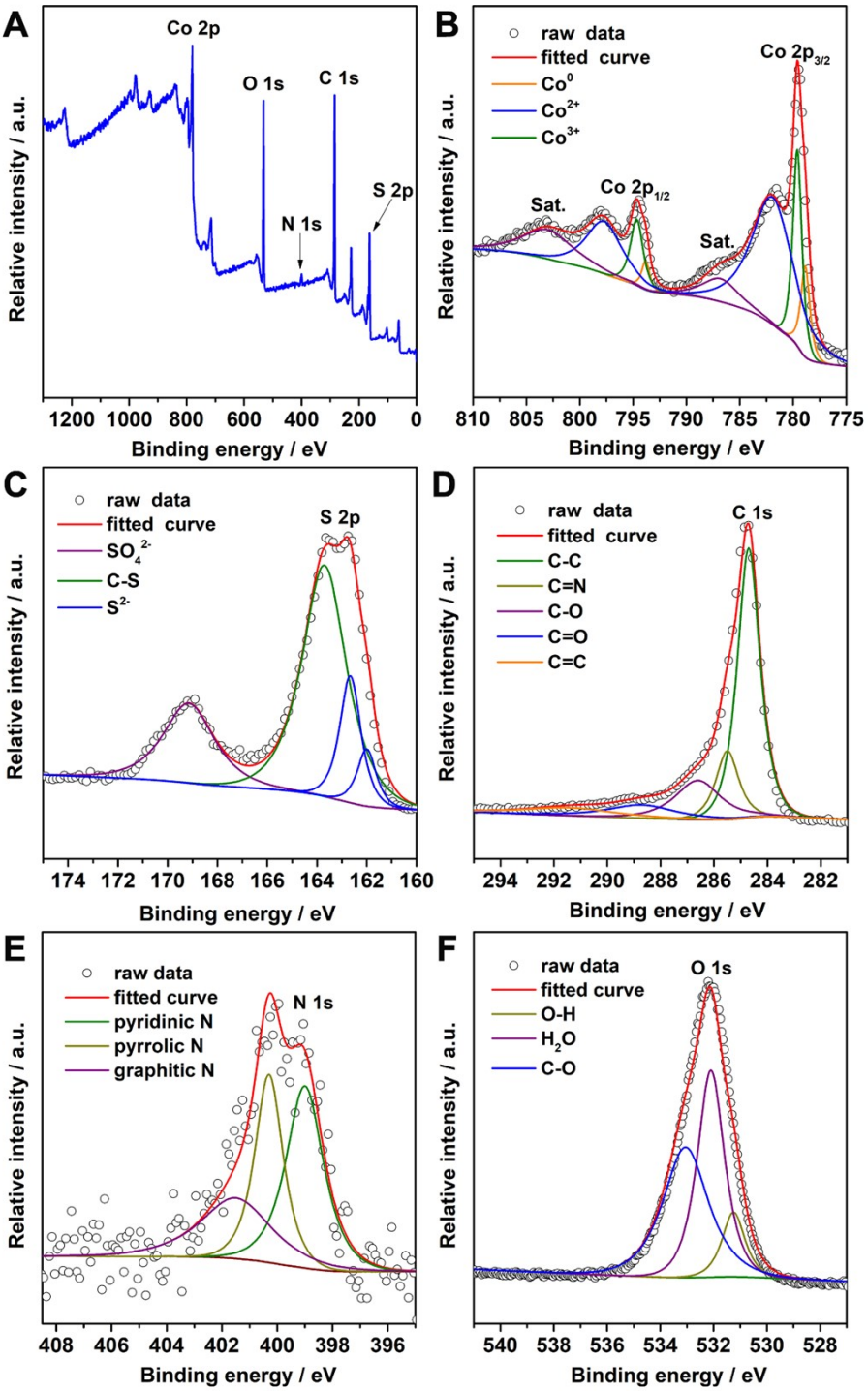

Fig. S8 (A-F) XPS survey spectrum and the high-resolution spectra of Co, S, C, N and O of the surface sulfurized Co-N-C/S (low DoS).

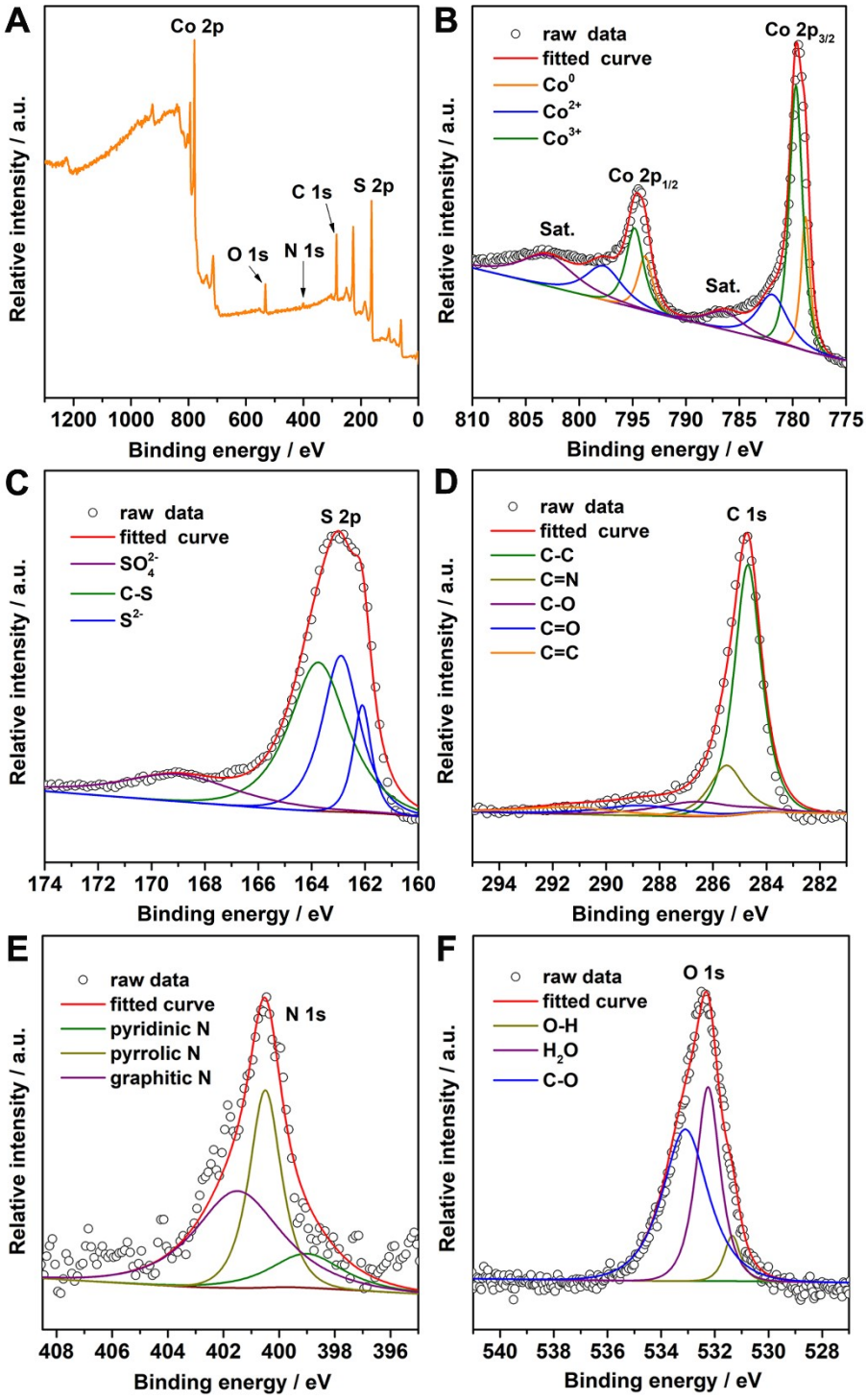

Fig. S9 XPS spectra of the partially sulfurized Co_3S_4/Co-N-C (medium DoS). (A) Survey spectrum. (B-F) Co, S, C, N and O spectra.

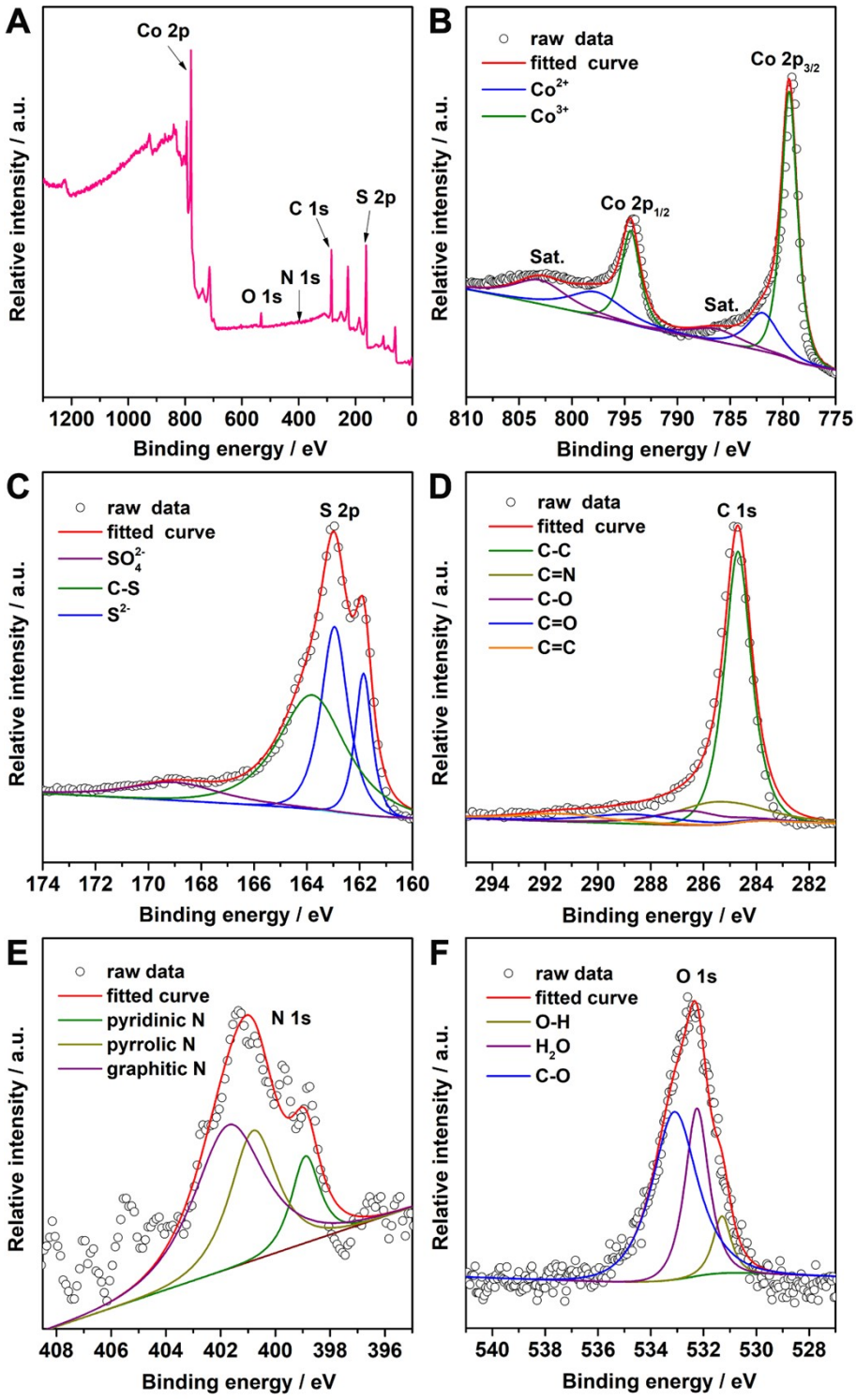

Fig. S10 (A-F) XPS survey spectrum and the high-resolution spectra of Co, S, C, N and O of the fully sulfurized Co_3S_4/N-C (high DoS).

Table S2 Comparison of the OER activity. All the data were obtained in O_2-purged 1 M KOH electrolyte.

	j_{geo}@1.7 V vs. RHE [mA cm^{-2}]	η@10 mA cm^{-2} [mV]	$j_{Cdl}@\eta_{400\ mV}$ [A F^{-1}]	$j_{BET}@\eta_{400\ mV}$ [mA cm_{BET}^{-2}]	Ref.
Co-N-C	37.6	395	1.8	0.014	this work
Co-N-C/S (low DoS)	62.1	339	4.5	0.061	this work
Co_3S_4/Co-N-C (medium DoS)	129.1	225	11.2	0.246	this work
Co_3S_4/N-C (high DoS)	78.1	316	5.4	0.129	this work
Co_3S_4/Co-N-C /I-t activation	296.6	---	19.3	---	this work
Co_3S_4/Co-N-C /1000 CV cycles	209.8	---	14.8	---	this work
CoO_x/N-C	41.1	352	---	0.029	11
Co/N-cage-in-cage porous carbon	30.0	401	---	---	12
Co_3S_4@$NiMoO_4$	50.9	320	0.4	0.044	13
CoP_2/Fe-CoP_2 yolk-shell nanobox	100.8	266	3.8	0.230	14
onion-like carbon /Co-N-C	~118	344	2.1	0.054	15
Mo-Co_3O_4/CNT	~80	280	4.4	0.191	16
graphene/MW CNT /Co-N-C_{800}	~103	357	1.4	---	17
carbon cloth /Co-N-C_{800}	~98	359	1.2	---	17
hydrophilic Co_3S_4	80.2	360	---	---	18
hydrophobic Co_3S_4	6.0	520	---	---	18

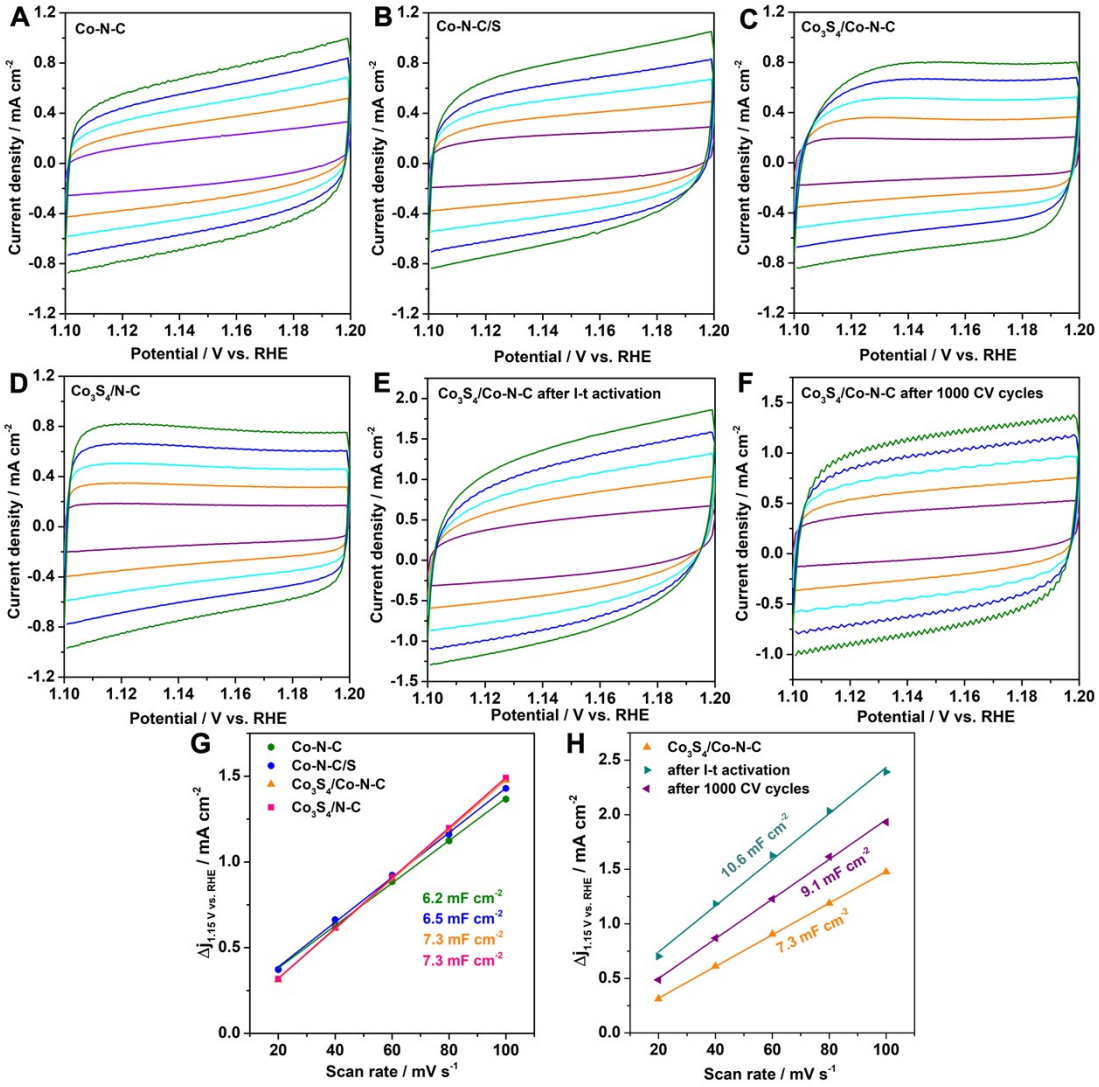

Fig. S11 Cyclic voltammetry curves measured in a non-redox region of 1.1-1.2 V vs. RHE. (A) Co-N-C, (B) surface sulfurized Co-N-C/S, (C) partially sulfurized Co_3S_4/Co-N-C, (D) fully sulfurized Co_3S_4/N-C, (E) Co_3S_4/Co-N-C after I-t activation and (F) Co_3S_4/Co-N-C after 1000 CV cycles. (G-H) The differences in current variation plotted against the scan rates to estimate the C_{dl} values.

The estimation of the effective active surface area was carried out according to literature.[19] Cyclic voltammetry (CV) were conducted at various scan rates (20, 40, 60, 80, 100 mV s^{-1}) in the region of 1.1-1.2 V vs. RHE where no redox reaction occurs (Fig. S11A-F), which can be considered as the double-layer capacitive behavior. The electrochemical double-layer capacitance (C_{dl}) of the catalysts can be identified from the

CV curves, which is expected to be linearly proportional to the electrochemically active surface area. The C_{dl} value is estimated by plotting the Δj (j_a-j_c) at 1.15 V vs. RHE against the scan rates, where the slope is twice C_{dl}. The C_{dl} values were listed in Fig. S11G-H.

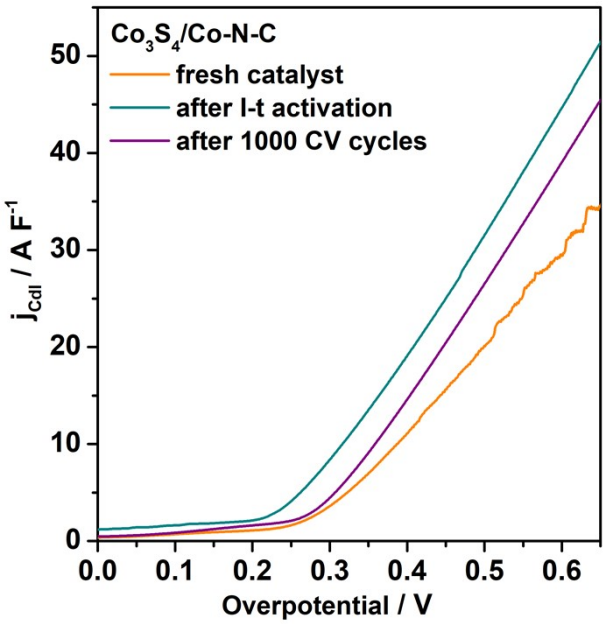

Fig. S12 Comparison of the C_{dl}-normalized LSV curves of Co_3S_4/Co-N-C before and after I-t and CV activation.

Based on the C_{dl} values of the activated Co_3S_4/Co-N-C catalyst, C_{dl}-normalization on the as-obtained LSV curves in Fig. 3B was conducted. As can be seen from Fig. S12, considerable increment of the C_{dl}-normalized activity can be revealed. At an overpotential of 0.4 V, the j_{Cdl} values reaches 19.3 and 14.8 A F^{-1} after I-t activation and 1000 CV cycles (Table S2), which exhibit 1.72 and 1.32 times enhancement that the fresh catalyst, further confirming the obviously improved intrinsic activity benefitted from the pre-oxidation process.

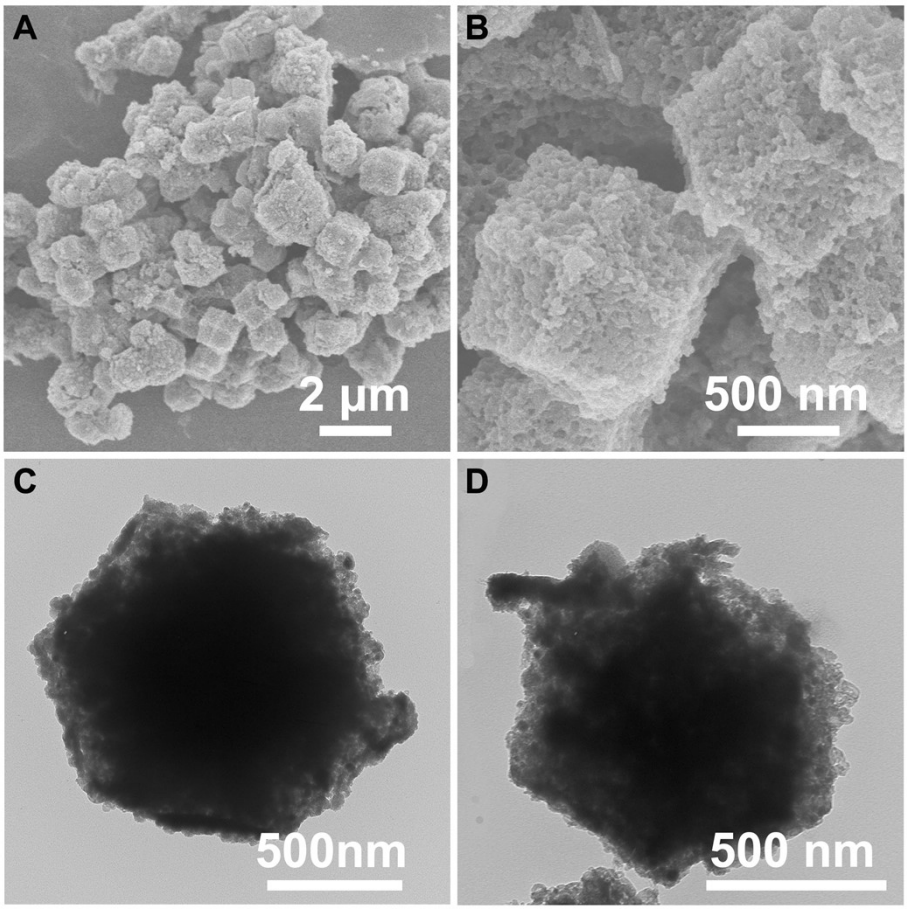

Fig. S13 (A-B) SEM and (C-D) TEM images of the partially sulfurized Co_3S_4/Co-N-C hybrid catalyst after continuous OER operation for 300 hours.

Reference

1. T. Wang, Z. Kou, S. Mu, J. Liu, D. He, I. S. Amiinu, W. Meng, K. Zhou, Z. Luo, S. Chaemchuen and F. Verpoort, *Adv. Funct. Mater.*, 2018, **28**, 1705048.
2. L. Gao, J. Xie, S. Liu, S. Lou, Z. Wei, X. Zhu and B. Tang, *ACS Appl. Mater. Interfaces*, 2020, **12**, 24701-24709.
3. W. Liu, J. Xie, Y. Guo, S. Lou, L. Gao and B. Tang, *J. Mater. Chem. A*, 2019, **7**, 24437-24444.
4. S. Wang, G. Zhou, J. Lv, Y. Ma, Y. Wang, C. Hu, J. Zhang, J. Yang, G. He, M. Zhang, M. Zhao, X. Chen and L. Yang, *J. Phys. Chem. Solids*, 2021, **148**, 109696.
5. T. Liu, P. Zhao, X. Hua, W. Luo, S. Chen and G. Cheng, *J. Mater. Chem. A*, 2016, **4**, 11357-11364.

6. B. Qiu, C. Yang, W. Guo, Y. Xu, Z. Liang, D. Ma and R. Zou, *J. Mater. Chem. A*, 2017, **5**, 8081-8086.
7. W. Zhang, X. Yao, S. Zhou, X. Li, L. Li, Z. Yu and L. Gu, *Small*, 2018, **14**, 1800423.
8. Y. Chen, S. Ji, Y. Wang, J. Dong, W. Chen, Z. Li, R. Shen, L. Zheng, Z. Zhuang, D. Wang and Y. Li, *Angew. Chem. Int. Ed.*, 2017, **56**, 6937-6941.
9. L. Li, L. Song, H. Guo, W. Xia, C. Jiang, B. Gao, C. Wu, T. Wang and J. He, *Nanoscale*, 2019, **11**, 901-907.
10. J. Xie, H. Qu, F. Lei, X. Peng, W. Liu, L. Gao, P. Hao, G. Cui and B. Tang, *J. Mater. Chem. A*, 2018, **6**, 16121-16129.
11. H. Zhou, M. Zheng, H. Tang, B. Xu, Y. Tang and H. Pang, *Small*, 2020, **16**, 1904252.
12. T. Wang, Y. He, Y. Liu, F. Guo, X. Li, H. Chen, H. Li and Z. Lin, *Nano Energy*, 2021, **79**, 105487.
13. L. Chen, G. C. Xu, G. Xu, L. Zhang and H. Ding, *Int. J. Hydrogen Energy*, 2020, **45**, 30463-30472.
14. V. Ganesan, J. Son and J. Kim, *Nanoscale*, 2021, **13**, 4569-4575.
15. Z. Liang, N. Kong, C. Yang, W. Zhang, H. Zheng, H. Lin and R. Cao, *Angew. Chem. Int. Ed.*, 2021, **60**, 12759-12764.
16. K. Lu, T. Gu, L. Zhang, Z. Wu, R. Wang and X. Li, *Chem. Eng. J.*, 2021, **408**, 127352.
17. Y. Zhang, H. Sun, Y. Qiu, X. Ji, T. Ma, F. Gao, Z. Ma, B. Zhang and P. Hu, *Carbon*, 2019, **144**, 370-381.
18. M. Zhu, Z. Zhang, H. Zhang, H. Zhang, X. Zhang, L. Zhang and S. Wang, *J. Colloid Interface Sci.*, 2018, **509**, 522-528.
19. J. Xie, J. Zhang, S. Li, F. Grote, X. Zhang, H. Zhang, R. Wang, Y. Lei, B. Pan and Y. Xie, *J. Am. Chem. Soc.*, 2013, **135**, 17881-17888.